Comparing visible-near-infrared spectroscopy and a pedotransfer function for predicting the dry region of the soil-water retention curve

Pittaki-Chrysodonta, Zampela; Arthur, Emmanuel; Moldrup, Per; Knadel, Maria; Norgaard, Trine; Iversen, Bo V.; De Jonge, Lis Wollesen

Published in:
Vadose Zone Journal

DOI (link to publication from Publisher):
10.2136/vzj2018.09.0180

Publication date:
2019

Document Version
Publisher's PDF, also known as Version of record

Published May 3, 2019

Original Research

Core Ideas

- The Campbell–Shiozawa (CS) model was fitted to dry region data.
- The CS model was anchored to soil water content at -10^6 cm H_2O matric potential.
- The model's parameters were well predicted from vis-NIR spectra or a PTF.
- Both the vis-NIRS and PTF models gave good predictions of dry region water retention.

Comparing Visible–Near-Infrared Spectroscopy and a Pedotransfer Function for Predicting the Dry Region of the Soil-Water Retention Curve

Zampela Pittaki-Chrysodonta,* Emmanuel Arthur, Per Moldrup, Maria Knadel, Trine Norgaard, Bo V. Iversen, and Lis Wollesen de Jonge

The soil-water retention curve (SWRC) at the dry end, also known as soil water vapor sorption isotherms, is essential for the modeling of water vapor transport, microbial activity, and biological processes such as plant water uptake in the vadose zone. Measurement of detailed soil water vapor sorption isotherms (WSIs) can be time consuming. Therefore, we propose rapid, inexpensive methodologies (visible–near-infrared spectroscopy [vis–NIRS] and a pedotransfer function [PTF]) to predict the Campbell–Shiozawa (CS) model parameters to obtain the WSIs. Water vapor sorption isotherms were measured on 144 soil samples with a vapor sorption analyzer. The CS semi-logarithmic-linear function anchored at a soil-water matric potential of -10^6 cm H_2O ($\log|-10^6| = pF\ 6$) was fitted to the measured data because it accurately characterizes the WSIs. Thereafter, a vis–NIRS calibration model and a PTF, based on clay and organic C contents, were developed and used to predict the two reference CS model parameters (α and W_6). Both parameters were predicted with a reasonable degree of accuracy using vis–NIRS and the PTF (for α, RMSE values of 0.0041 and 0.0025, and for W_6, RMSE values of 0.0042 and 0.0034 for vis–NIRS and the PTF, respectively). Based on the predicted α and W_6 values, the predicted WSIs compared closely with the measured isotherms for individual soil samples from each field. At the field scale, the vis–NIRS model performed marginally better than the PTF. Thus, it is evident that the use of vis–NIRS or PTFs provides a relatively inexpensive approach to predicting soil water sorption isotherms.

Abbreviations: CS, Campbell–Shiozawa; NIR, near-infrared; OC, organic carbon; PLS, partial least squares; PTF, pedotransfer function; RMSEC, root mean square error of calibration; RMSECV, root mean square error of cross-validation; RPIQ, ratio of performance to interquartile distance; SWRC, soil-water retention curve; vis–NIRS, visible near-infrared spectroscopy; WSI, water vapor sorption isotherm.

The dry end of a soil-water retention curve (SWRC), which describes the water content at low matric potentials (less than −10 MPa) is important for understanding and modeling water transport and biochemical processes in the vadose zone. Several mechanistic and empirical models have been proposed in the literature to accurately describe the SWRC under wet and dry conditions (Brunauer et al., 1938; Oswin, 1946; van Genuchten, 1980; van den Berg and Bruin, 1981; Campbell and Shiozawa, 1992; Peleg, 1993; Rossi and Nimmo, 1994; Or and Tuller, 1999; Tuller and Or, 2005). Furthermore, Khlosi et al. (2008) evaluated eight SWRC functions that characterize the SWRC between saturation and oven dryness. Ciocca et al. (2014) studied the effects of infinitely negative matric potentials at residual water content on the negative atmospheric fluxes from arid soils and emphasized how a more sufficient experimental characterization of water retention close to and below the residual water content will be valuable. However, the simplest among these models is the semi-logarithmic Campbell–Shiozawa (Campbell and Shiozawa, 1992) (denoted hereafter as the CS function), which requires only knowledge of the dimensionless slope of the curve (α) and the matric potential at oven dryness (Ψ_0). The intercept ($pF_0 = \log_{10}|\Psi_0|$) of the CS function has a narrow

Z. Pittaki-Chrysodonta, E. Arthur, M. Knadel, T. Norgaard, B.V. Iversen, L.W. de Jonge, Dep. of Agroecology, Faculty of Science and Technology, Aarhus Univ., Blichers Alle 20, P.O. Box 50, DK-8830 Tjele, Denmark; P. Moldrup, Dep. of Civil Engineering, Aalborg Univ., Thomas Manns Vej 23, DK-9220 Aalborg, Denmark.*Corresponding author (zambella.pittaki@agro.au.dk).

Received 19 Sept. 2018.
Accepted 29 Jan. 2019.

Citation: Pittaki-Chrysodonta, Z., E. Arthur, P. Moldrup, M. Knadel, T. Norgaard, B.V. Iversen, and L.W. de Jonge. 2019. Predicting the Campbell–Shiozawa soil-water retention function for the dry region: Comparing visible–near-infrared spectroscopy with a classical pedotransfer function. Vadose Zone J. 18:180180. doi:10.2136/vzj2018.09.0180

range, and many researchers consider it as constant (~6.7–7.1) (Groenevelt and Grant, 2004; Schneider and Goss, 2012; Arthur et al., 2013). However, other studies have shown that it can be variable depending on the clay mineralogy (Lu and Khorshidi, 2015; Karup et al., 2017). Measuring the dry end of the SWRC is a time-consuming process, and thus a fast method is needed for easy predictions within an acceptable range of errors. A detailed dry-end SWRC at various matric potentials can be achieved using instruments that are based on chilled mirror dew point technology (e.g., WP4-T potentiometer, and the fully automated vapor sorption analyzer) (Arthur et al., 2014a).

During the last decades, many researchers have developed functions to predict the dry-end SWRC using basic soil properties (e.g., clay content). Karup et al. (2017) predicted the water content at -10^6 cm H_2O ($\log_{10}|-10^6|$ = pF 6) using the clay content, organic matter, and silt fraction as well as the bulk density coupled with the assumption of linearity between pF 4.2 and pF 6.9. Schneider and Goss (2012), based on 18 samples, showed that the dry end of the SWRC can be successfully predicted from a PTF based on clay content. Utilization of PTFs is an easy method to estimate the SWRC, but the required data (e.g., clay, organic C, silt, etc.) are still expensive and tedious to acquire.

Visible near-infrared spectroscopy (vis–NIRS) is a fast, nondestructive method that has received increasing attention during the last few decades, mainly due to its simplicity and low cost. It is a spectroscopic method that uses the visible and near-infrared regions of the electromagnetic spectrum (400–2500 nm). The radiation causes individual molecular bonds in the soil to vibrate and absorb light with a specific energy quantum (Stenberg et al., 2010). Visible-NIRS has been applied to predict different soil properties including basic soil properties such as soil organic C, clay, and water content (Stenberg et al., 2010). However, more recently the capability of the method to successfully predict other soil properties was also tested in studies on particle size distribution (Hermansen et al., 2017), soil structure (Katuwal et al., 2017), soil binding capacities (Paradelo et al., 2016), and water repellency (Knadel et al., 2016). Furthermore, vis–NIRS models have been developed to predict the wet end of the soil water retention curve (Santra et al., 2009; Babaeian et al., 2015; Pittaki-Chrysodonta et al., 2018). Despite the potential of vis–NIRS to predict direct or indirect soil properties and processes, there is no existing research that attempts to predict the dry end of a SWRC using vis–NIRS.

The objective of this study was to examine whether vis–NIRS can be used as a tool for predicting the SWRC at the dry end equally well as a classical PTF.

Material and Methods

Soil Samples

Bulk soil samples (144) from different countries with different textures were used in this study (Fig. 1a). The soils were sampled from the 0- to 20-cm depth (topsoils) in Denmark (DK),

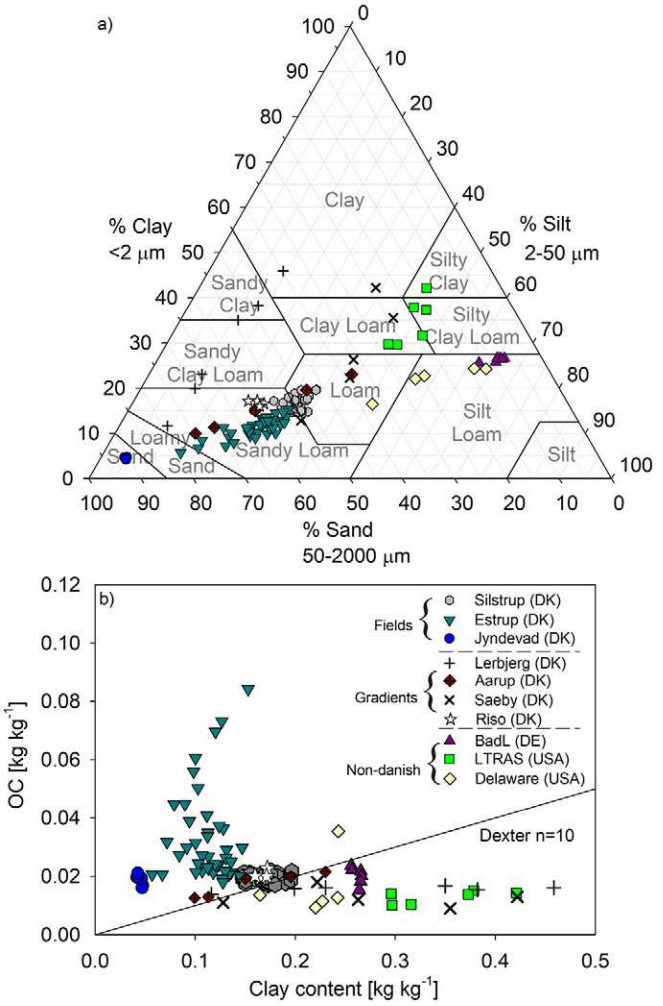

Fig. 1. (a) Distribution of the soil samples in the USDA soil texture triangle, and (b) organic C (OC) content as a function of clay content for all soil samples. Dexter *n* indicates the ratio of clay content to OC.

Germany (DE), and the United States (USA). Specifically, the soil samples from Denmark were sampled in Silstrup (60 soil samples), Estrup (41), Jyndevad (6), Lerbjerg (5), Aarup (5), Saeby (5), and Riso (4). The sites of Silstrup (56°55′ N, 8°38′ E), Estrup (56°29′ N, 9°4′ E) and Jyndevad (54°53′ N, 9°7′ E) are part of the Danish Pesticide Leaching Assessment Program and are representative sites covering a variety of soil types in Denmark. The sampling at these sites was performed on a 15- by 15-m grid to capture across-field variations. More information about the soils from Silstrup, Estrup, and Jyndevad can be found in Norgaard et al. (2013), Paradelo et al. (2015), and Masís-Meléndez et al. (2014), respectively. Six soil samples were obtained from Bad Lauchstädt (BadL) (51°24′ N, 11°53′E) in the central part of Germany. Detailed information for that site was described by Eden et al. (2012). The soil samples from the United States originated from the Long-Term Research on Agricultural Systems (LTRAS) project at the University of California, Davis, and from the University of Delaware (six and five soils, respectively). Both sites were described by Vendelboe et al. (2012).

Measurements

All the measurements were performed on air-dried soil samples sieved to 2 mm. The particle-size fractions (USDA soil textural classification) were determined using a combination of wet sieving and the hydrometer method (Gee and Or, 2002). Total organic C (OC) was determined with a Flash 2000 organic elemental analyzer coupled with a thermal conductivity detector (Thermo Scientific) and converted to organic matter (OM) by multiplying by 1.72.

Soil water vapor desorption isotherms were measured for the water activity (a_w) range from 0.03 to 0.93 with a 0.02 resolution at a temperature of 25°C with a fully automated AquaLab vapor sorption analyzer (METER). The vapor sorption analyzer dries or wets an air-dry soil sample with a chilled-mirror dew-point technique and simultaneously records the change in sample mass with a high-precision magnetic balance. Approximately 3 to 5 g of the 2-mm sieved and air-dried sample of each soil was used without any pretreatment. A more detailed description of the measurements was provided by Arthur et al. (2014b). The values of a_w were converted to soil water potentials using the well-known Kelvin equation:

$$\Psi_w = \frac{RT}{M_w}\ln(a_w) \quad [1]$$

where Ψ_w is the soil water potential, R is the universal gas constant (8.314 J mol^{-1} K^{-1}), T is temperature (298.15 K or 25°C), and M_w is the molecular mass of water (0.018 kg mol^{-1}). Since none of the samples contained significant amounts of salts, the osmotic potential was negligible and the soil water potential equals the matric potential.

The vis–NIRS (400–2500 nm) measurements with a 0.5-nm spectral interval were performed using approximately 50 g of the representative soil sample. The soil sample was placed in a 60-mm sampling cup and the reflectance in the vis–NIRS range was measured using a NIRS DS2500 spectrometer (FOSS) in a temperature- and humidity-controlled NIR laboratory (23°C and 48%, respectively). The instrument has two detectors: silicon (400–1100 nm) and lead sulfide (1100–2500 nm). The measurements of the reflectance were taken in seven positions of the sampling cup, and the averaged spectrum was extracted for each soil. Reflectance measurements were transformed to apparent absorbance by log(reflectance^{-1}).

Campbell–Shiozawa Function Anchored at pF 6

The CS function is a simple semi-linear equation that predicts the logarithm of the soil water matric potential ($\log_{10}|-\psi|$ = pF) at a given soil water content (W), and therefore it is called the log-linear CS function:

$$\mathrm{pF} = \mathrm{pF}_0 - \alpha W \quad [2]$$

or

$$W = \alpha^{-1}(\mathrm{pF}_0 - \mathrm{pF}) \quad [3]$$

where W is the gravimetric water content (g g^{-1}), pF is the logarithm of the soil water matric potential, pF_0 is the logarithm of the soil water matric potential under oven-dry conditions (W = 0) being equal to the intercept of the log-linear function, and α is the negative slope (dimensionless) of the log-linear scale ($\log_{10}|-\psi|$ vs. W system).

A number of studies used a constant value at pF_0 (W = 0, pF_0) of 6.7 to 7.1 (Ross et al., 1991; Rossi and Nimmo, 1994; Fayer and Simmons, 1995; Webb, 2000; Groenevelt and Grant, 2004; Schneider and Goss, 2012; Arthur et al., 2013). Since studies have shown that pF_0 can be variable depending on the clay mineralogy or cation exchange capacity (Lu and Khorshidi, 2015; Karup et al., 2017), we anchored the CS function instead at the gravimetric soil water content at -10^6 cm H_2O (W_6, pF = 6). Consequently, the two parameters in the CS function became W_6 and α, and therefore, the modified CS function can be expressed as

$$W = W_6 + \alpha^{-1}(6 - \mathrm{pF}) \quad [4]$$

or

$$\mathrm{pF} = \alpha(W - W_6) + 6 \quad [5]$$

The equation is in a linear form and thus the measurements of soil water desorption isotherms on a log-linear scale should produce a straight line. However, this linearity was observed to be valid for the a_w range from 0.1 to 0.8 (or pF 6.5–5.5), and therefore the analysis includes only measurements in that range. Additionally, the desorption isotherms were measured initially by adsorption followed by desorption with a range of 0.03 to 0.93. As a consequence, the ends of the isotherm branches bend and lose linearity due to the measurement settings. Therefore, in the selected range (0.1–0.8), the problem of nonlinearity of the measurements is avoided. Hysteresis phenomena exist for water vapor sorption–desorption isotherms (Arthur et al., 2015; Lu and Khorshidi, 2015) and, as we considered only desorption isotherms, our results may not be applicable to adsorption isotherms.

Figure 2 depicts measurements of WSI for a soil (Estrup) and schematically illustrates the calculation of the reference parameters α, W_6, and pF_0 in the CS functions (original and anchored). Furthermore, it shows an example of the fitting of the original CS function as well as the anchored CS function to the measured data.

Multivariate Data Analysis

The two reference parameters of the CS function (α and W_6) for each soil sample were correlated with the spectral measurements using partial least squares (PLS) regression analysis with the straight forward implementation of a statistically inspired modification of the PLS (SIMPLS) algorithm (de Jong, 1993). The PLS regression method compresses the predictors (independent variables) into a set of factors (or latent variables) and applies least square regression on these factors. The SIMPLS algorithm directly calculates the PLS factors as linear combinations of the original variables (de Jong, 1993). The analysis was performed using the software PLS Toolbox 8.6.1 (Eigenvector Research). The vis–NIRS models were validated using the venetian blind cross-validation method with 10 split groups and one sample per split

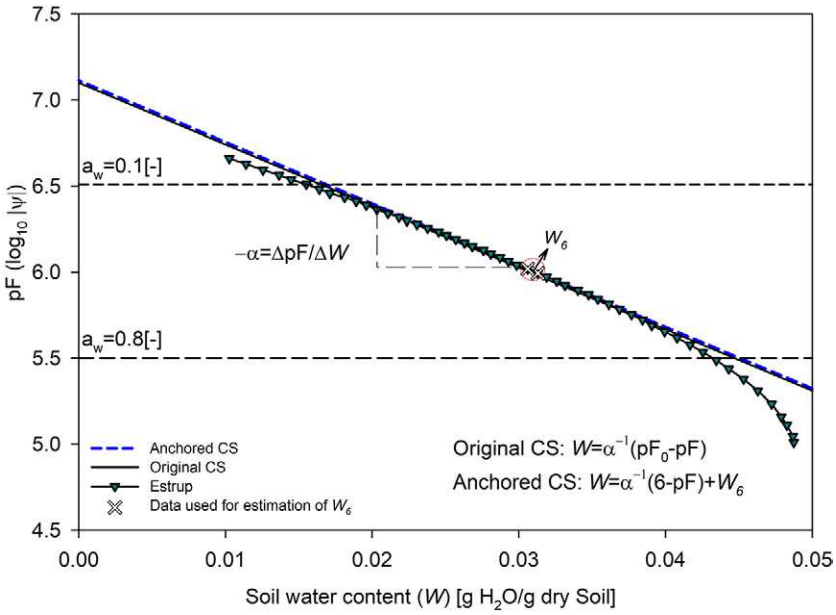

Fig. 2. Schematic illustration of the calculation of the two reference parameters α and W_6 for a soil sample, as well as the fitting of the original and anchored Campbell–Shiozawa (CS) functions at the selected range (relative humidity 0.1–0.8), where α is the slope of the log-linear Campbell–Shiozawa function, W_6 is the gravimetric water content at -10^6 cm H_2O, and a_w is the water activity.

(Snee, 1977). The most desirable way of validating the models is using an independent data set. However, due to the geographic origin of the investigated soils, it was not possible to split the data set into calibration and validation subsets. The soils originated from fields or from point samples (individual soils sampled in a small area) at different locations, representing very different geology. As previously reported, the validation procedure performed using soils of a different geographic origin and geology than of those used in the calibration is problematic and leads to increased errors and bias (Reeves et al., 1999; Brown et al., 2005).

To improve the spectra quality and to find the best correlation among spectral measurements and reference data (α and W_6), different preprocessing techniques were applied, i.e., derivatives (Savitzky and Golay, 1964; Norris, 2001) and standard normal variate transformation and detrending (Barnes et al., 1989).

The quality of the vis–NIRS models was examined via the following statistical parameters: R^2, which is the square of the Pearson correlation coefficient, RMSE of calibration (RMSEC), RMSE of cross-validation (RMSECV), and the ratio of performance to interquartile distance (RPIQ). The RMSEC and RMSECV are defined as

$$\mathrm{RMSE} = \sqrt{\frac{1}{N}\sum_{i=1}^{N}\left(\hat{y}_i - y_i\right)^2} \qquad [6]$$

where N is the number of samples, $\hat{y}_i$ is the predicted values and y_i is the measured value. When the predicted values are derived from the calibration and cross-validations data, then the RMSE corresponds to the RMSEC and RMSECV, respectively.

The RPIQ is an index based on the interquartile range (IQ = Q3–Q1) and therefore represents the spread of the dataset regardless of its distribution (Bellon-Maurel et al., 2010). The Q1 is the first quartile, which is the median of the lower half of the dataset, and Q3 is the third quartile, which is the median of the upper half of the dataset:

$$\mathrm{RPIQ} = \frac{\mathrm{IQ}}{\mathrm{SEP}} \qquad [7]$$

where IQ is a measure of statistical dispersion around the median and SEP is the standard error (SE) of prediction, which was replaced by RMSECV in this study.

The optimum number of factors was identified as the local minimum value of the RMSEC and RMSECV where the slope did not decrease significantly (Gowen et al., 2011). It is important that the number of factors is not too significantly higher or lower than the optimum because that will lead to an over- or underestimation, respectively, of the models.

Pedotransfer Function

Several PTFs have been developed to predict the SWRC (wet or dry part) or water content at a given matric potential from soil properties such as clay content, organic matter, and bulk density (Campbell and Shiozawa, 1992; Schneider and Goss, 2012; Wuddivira et al., 2012; Arthur et al., 2013, 2015; Chen et al., 2014; Karup et al., 2017). The studies of Arthur et al. (2013) and Schneider and Goss (2012) provided PTFs for estimating the inverse of the CS slope with only the clay content. Both studies considered the intercept (pF_0) of the log-linear CS function as constant. Jensen et al. (2015) correlated the volumetric water content at -10^6 cm H_2O (pF 6) with clay content, OM, silt, and bulk density. The PTF of Wuddivira et al. (2012) predicted clay content using water content at a relative humidity of 0.5, which corresponds to a matric potential of -10^6 cm H_2O. To predict the reference slope of the CS function, the inverse of α was used because previous studies correlated it to the soil properties (Schneider and Goss, 2012; Arthur et al., 2013). To develop PTFs for the two reference parameters, α and W_6, in the current study, the following regression models were used:

$$\alpha^{-1} = A \times \text{Clay} + B \times \text{OM} \quad [8]$$

$$W_6 = C \times \text{Clay} + D \times \text{OM} \quad [9]$$

where Clay is the clay content (kg kg^{-1}), OM is organic matter (kg kg^{-1}), and A, B, C, and D are the regression coefficients. The evaluation of both PTFs was performed using the R^2, RMSE, and RPIQ indices.

Comparison of Visible–Near-Infrared Spectroscopy and Pedotransfer Function

The statistical evaluations of the two methods were compared to examine the overall model accuracy and to examine if vis–NIRS can predict the SWRC at the dry end. Additionally, the predicted parameters were inserted into the anchored log-linear CS function and the dry-end SWRCs of individual soil samples were predicted using either the vis–NIRS calibration models or the PTF. The ability to predict the dry-end SWRC on a field scale was also tested using the two available fields (Silstrup and Estrup).

Results and Discussion

Soil Properties and Water Vapor Sorption Isotherms

The soil samples used in this study covered a wide textural range (11 USDA soil texture classes) as illustrated in Fig. 1a. The mean values (with range in parentheses) of R^2 and RMSE of the fits of the anchored CS model to the measured water desorption isotherms, WSIs (0.1–0.8 a_w), were 0.998 (0.980–1.000) and 0.012 (0.0004–0.039) g g^{-1}, respectively. The descriptive statistics of the clay content, OC, and the two reference parameters of the anchored log-linear CS function (α and W_6) of all 10 datasets are presented in Table 1. The clay content and OC ranged from 0.04 to 0.46 and 0.009 to 0.084 kg kg^{-1}, respectively. The reference slope (α) and the gravimetric water content at pF6 (W_6) varied from 16.71 to 165.54 (dimensionless) and 0.009 to 0.060 g g^{-1}, respectively. Higher absolute values of the reference α indicate sandier soils, while lower values indicate more clayey soils.

The soil samples from Silstrup varied from sandy loam to loam, with a narrow textural distribution, while the samples from Estrup ranged from loamy sand to sandy loam. All samples from Jyndevad were characterized as sands. The soil samples from Lerbjerg, Aarup, Saeby, and Riso had a wide textural range covering six classes (sandy loam, loam, clay loam, sandy clay loam, sandy clay, and clay). Samples from Germany (BadL) were characterized as silt loam, while soil samples from the United States (LTRAS and Delaware) had a wide textural distribution across the soil texture triangle (Fig. 1a), covering five classes (clay loam, silty clay loam, and silty clay for LTRAS and loam and silty loam for Delaware).

The reference α values for the Silstrup samples varied between 42.60 and 59.86 (narrow distribution), while for Estrup it was 35.80 and 105.45, with average values of 51.05 and 63.10, respectively, for the two fields. The W_6 values ranged from 0.015 to 0.023 ($\overline{W}_6$ = 0.020) and 0.009 to 0.031 ($\overline{W}_6$ = 0.016) g g^{-1} for Silstrup and Estrup, respectively.

Table 1. Statistical characteristics of clay content, organic C (OC), and the two reference parameters, the inverse of the slope of the Campbell–Shiozawa function (α^{-1}) and the gravimetric water content at -10^6 cm H_2O (W_6), of the anchored Campbell–Shiozawa (CS) model of each dataset.

Dataset	Statistic†	Clay	OC	α	W_6
		kg kg^{-1}			g g^{-1}
Silstrup (DK) (N = 60)	mean	0.16	0.020	51.05	0.020
	median	0.16	0.020	51.68	0.020
	Q1	0.15	0.019	49.33	0.019
	Q3	0.17	0.020	53.61	0.021
	σ	0.01	0.001	3.40	0.002
	range	0.15–0.20	0.017–0.022	42.60–59.86	0.015–0.023
Estrup (DK) (N = 41)	mean	0.11	0.033	63.10	0.016
	median	0.11	0.027	63.92	0.015
	Q1	0.10	0.022	55.32	0.013
	Q3	0.13	0.037	70.43	0.018
	σ	0.02	0.016	13.87	0.005
	range	0.06–0.15	0.018–0.084	35.80–105.45	0.009–0.031
Jyndevad (DK) (N = 6)	mean	0.04	0.019	136.48	0.011
	median	0.04	0.020	133.23	0.012
	Q1	0.04	0.018	116.84	0.010
	Q3	0.05	0.020	156.52	0.012
	σ	0.00	0.002	23.61	0.002
	range	0.04–0.05	0.016–0.021	111.19–165.54	0.009–0.013
Lerbjerg (DK) (N = 6)	mean	0.29	0.016	40.95	0.032
	median	0.29	0.016	34.89	0.029
	Q1	0.21	0.016	24.15	0.021
	Q3	0.37	0.016	47.46	0.041
	σ	0.13	0.001	25.62	0.017
	range	0.12–0.46	0.014–0.017	16.71–87.02	0.013–0.060
Aarup (DK) (N = 5)	mean	0.16	0.017	80.31	0.016
	median	0.15	0.019	77.18	0.015
	Q1	0.11	0.013	54.78	0.011
	Q3	0.20	0.020	107.58	0.021
	σ	0.06	0.004	28.39	0.006
	range	0.10–0.23	0.013–0.022	50.86–111.17	0.011–0.023
Saeby (DK) (N = 5)	mean	0.28	0.013	44.04	0.024
	median	0.26	0.012	41.91	0.022
	Q1	0.22	0.011	28.69	0.020
	Q3	0.36	0.013	46.54	0.029
	σ	0.11	0.003	20.75	0.009
	range	0.13–0.42	0.009–0.018	25.40–77.64	0.012–0.035

continued on next page.

Table 1. continued from previous page.

Dataset	Statistic†	Clay	OC	α	W_6
		—— kg kg^{-1} ——			g g^{-1}
Riso (DK) (N = 4)	mean	0.17	0.021	55.11	0.016
	median	0.17	0.020	54.89	0.016
	Q1	0.16	0.020	54.69	0.016
	Q3	0.17	0.021	55.31	0.016
	σ	0.01	0.001	0.86	0.001
	range	0.16–0.17	0.020–0.023	54.33–56.34	0.015–0.06
BadL (DE) (N = 6)	mean	0.26	0.020	36.51	0.029
	median	0.26	0.021	36.53	0.028
	Q1	0.26	0.019	35.33	0.028
	Q3	0.27	0.022	37.43	0.030
	σ	0.00	0.003	1.34	0.001
	range	0.26–0.27	0.015–0.024	35.03–38.30	0.027–0.030
LTRAS (USA) (N = 6)	mean	0.35	0.013	25.35	0.043
	median	0.34	0.014	25.86	0.043
	Q1	0.30	0.011	24.00	0.041
	Q3	0.38	0.014	26.74	0.045
	σ	0.05	0.002	1.91	0.004
	range	0.30–0.42	0.010–0.015	22.61–27.32	0.039–0.049
Delaware (USA) (N = 5)	mean	0.22	0.017	58.14	0.016
	median	0.23	0.013	57.26	0.014
	Q1	0.22	0.012	52.10	0.014
	Q3	0.24	0.014	62.33	0.016
	σ	0.03	0.011	12.88	0.005
	range	0.16–0.24	0.009–0.035	42.12–76.90	0.012–0.024
Total (N = 144)	mean	0.17	0.023	57.08	0.020
	median	0.15	0.020	52.73	0.019
	Q1	0.12	0.018	47.20	0.015
	Q3	0.18	0.022	61.46	0.022
	σ	0.08	0.011	22.95	0.008
	range	0.04–0.46	0.009–0.084	16.71–165.54	0.009–0.060

† Q1, first quartile of the dataset; Q3, third quartile of the dataset; σ, standard deviation of the dataset.

Figure 1b represents the variations in OC for all soils. The soil samples are grouped in two categories based on the ratio of clay content to OC (n), with a threshold value of n = 10 as suggested by Dexter et al. (2008). The n value can be used for grouping soils because it determines the amount of complexed clay controlling the physical properties and processes (de Jonge et al., 2009).

Examples of eight WSIs are depicted in Fig. 3. Two soil samples from each subplot are presented for (a) a sandy loam (Estrup) and sand-textured (Jyndevad) sample, (b) soils from the same dataset (BadL) with the same clay content (0.26 kg kg^{-1}) but with different OC contents (0.024 and 0.015 kg kg^{-1}), (c) soils derived from the same dataset (LTRAS) with equal contents of OC (0.014 kg kg^{-1}) but with different clay contents (0.42 and 0.30 kg kg^{-1}), and (d) soils with similar contents of OC (0.015 and 0.016 kg kg^{-1}) and almost twice the clay content (0.38 and 0.20 kg kg^{-1}). Thus, higher values of clay content and OC indicated higher values of desorbed soil water content, as the water molecules are retained on the surfaces, and clay content and OC are the largest contributors to the soil-specific surface area.

Visible–Near-Infrared Spectroscopy Measurements

Figure 4 illustrates the spectral behavior of four different soil samples, two samples with high and low reference α values and two samples with high and low reference W_6 values. The sandy soil from Jyndevad with the higher α value had clay and OC contents of 0.04 and 0.020 kg kg^{-1}, respectively, while the silty clay soil from LTRAS with lower α value had the respective contents equal to 0.42 and 0.014 kg kg^{-1}. The loamy sand soil from Estrup with the lower value of W_6 had clay and OC contents of 0.06 and 0.021 kg kg^{-1}, respectively, and the clayey Lerbjerg soil with a high value of W_6 had clay and OC contents of 0.46 and 0.016 kg kg^{-1}. Therefore the soil samples with high α and low W_6 represent low fine minerals and showed higher absorbance throughout the vis–NIRS range. Also, these two soil samples had the highest OC contents among the four selected soils and for that reason higher absorbance in the visible range compared with other two soil samples. Based on Galvão and Vitorello (1998), higher values of OC would lead to higher absorbance in the range from 600 to 750 nm. The peak around 1400 nm could be due to the first overtone of O–H stretch, while the peak near 1900 nm from OH bonds is due to a combination of vibrations of water bound in the interlayer lattice. The peak at 2200 nm could be assigned to the combination of OH stretch with the fundamental Al–OH bending mode (Hunt, 1977). The peaks related to OH bonds are the most pronounced for the Lerbjerg soil due to the high clay content.

Partial Least Squares Regression Analysis

The pretreatment method that resulted in the best calibrated models for both reference parameters (α^{-1} and W_6) was the gap segment (Norris, 2001) first derivative among the tested pretreatment methods. In the gap segment method, the derivative is calculated using multiple points in each segment, and the segments are separated by a number of points (non-zero values). The number of segments is defined by the order of the derivative (e.g., first derivative). Figure 5 illustrates the RMSEC, RMSECV, and the cumulative Y variance captured as a function of the number of factors in the PLS regression. The optimum number of factors was set to five for both vis–NIRS models. The R^2 of the calibrated models (R^2Cal), R^2 of the cross-validation (R^2CV), the RMSECV, and RPIQ are presented in Table 2. The R^2Cal, R^2CV, RMSECV, and RPIQ were 0.76, 0.72, 0.0041, and 0.93, respectively, for vis–NIRS-predicted α^{-1} and 0.76, 0.74, 0.0042, and 0.92, respectively, for W_6. The vis–NIRS-predicted values of α^{-1} and W_6 from the cross-validation are illustrated in Fig. 6. In Table 3, the statistical characteristics of the two vis–NIRS-predicted parameters for the

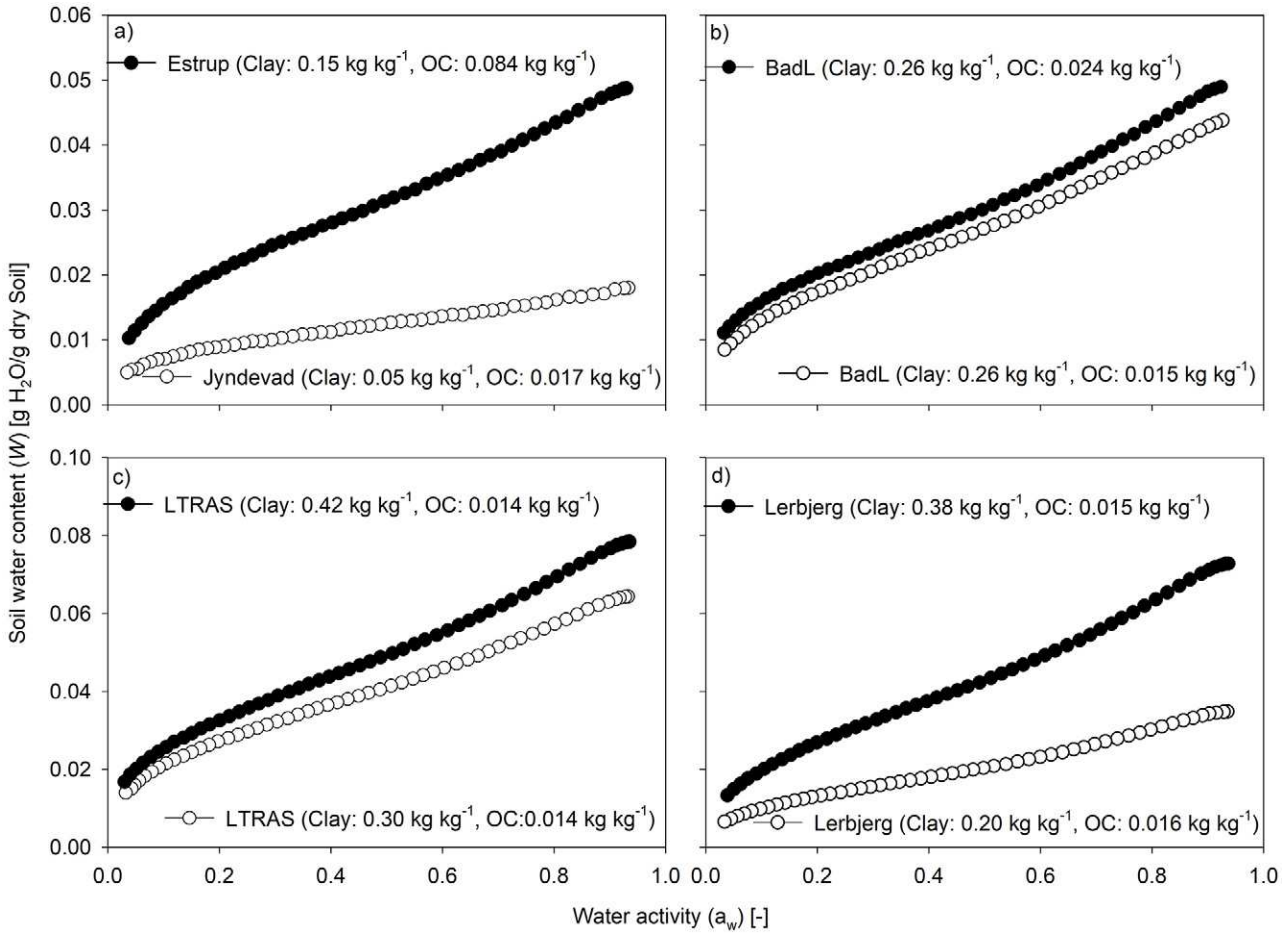

Fig. 3. Measured water vapor desorption isotherms for eight different soil samples: (a) a loamy sand (Estrup) and a sand (Jyndevad), and two soil samples from the same area but with different (b) organic C (OC) contents (BadL) and (c,d) clay (CF) contents (LTRAS and Lerbjerg, respectively).

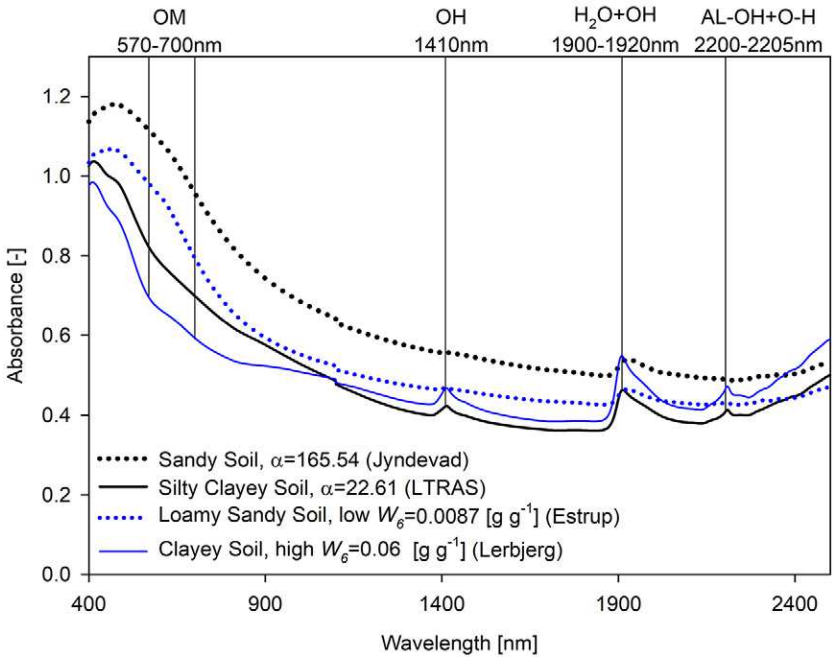

Fig. 4. Visible–near-infrared spectra of selected soil samples and the possible spectrally active components for a sand and a silty clay sample with high and low values of the reference slope (α) of the Campbell–Shiozawa function and for a loamy sand sample and a clay sample with low and high values of reference gravimetric water content at -10^6 cm H_2O (W_6), respectively; OM is organic matter.

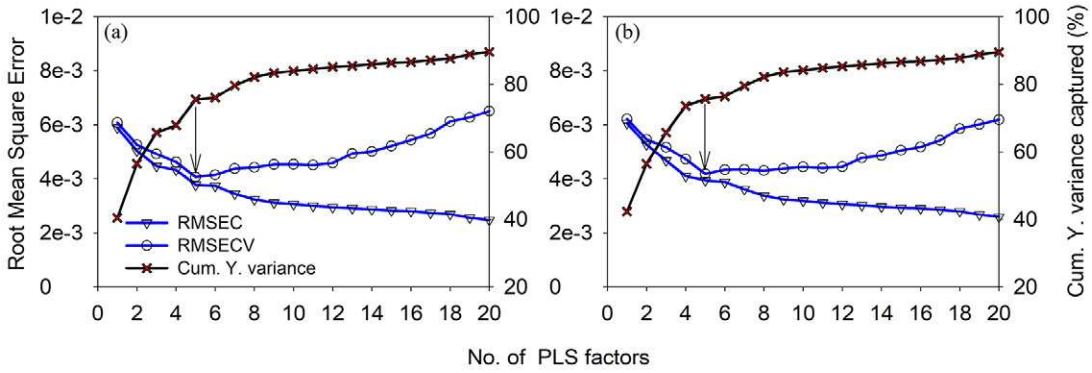

Fig. 5. Root mean square error of the calibration with the blue line (RMSEC) and cross-validation with the blue line (RMSECV) and cumulative Y variance captured as a function of the number of factors in the partial least squares (PLS) regression. The arrow indicates the selected number of factors used in the models: (a) for the inverse of the slope of the Campbell–Shiozawa function (α^{-1}) and (b) for the gravimetric water content at -10^6 cm H_2O (W_6).

entire database are presented. The mean measured value of α was 57.08 and the predicted value was 55.04, while the median, Q1, and Q3 values were approximately the same. The reference and predicted values of α ranged from 16.71 to 165.54 (σ = 22.95) and 19.47 to 178.72 (σ = 18.24), respectively. The statistical characteristics between the reference and predicted values of W_6 were almost identical and ranged from 0.009 to 0.060 and 0.008 to 0.052 g g^{-1}, respectively.

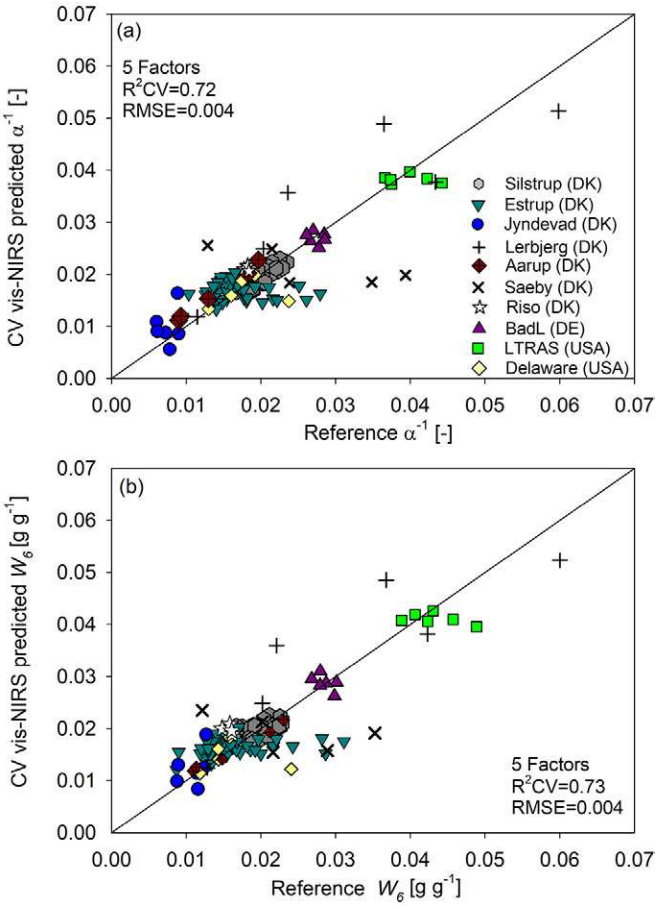

Fig. 6. Scatterplot of cross-validated visible–near-infrared spectroscopy (CV vis–NIRS) predicted and reference values of (a) inverse of the slope of the Campbell–Shiozawa function (α^{-1}) and (b) gravimetric water content at -10^6 cm H_2O (W_6). Also given are the number of factors, R^2 of the cross-validation (R^2CV), and the root mean square error of cross-validation (RMSECV).

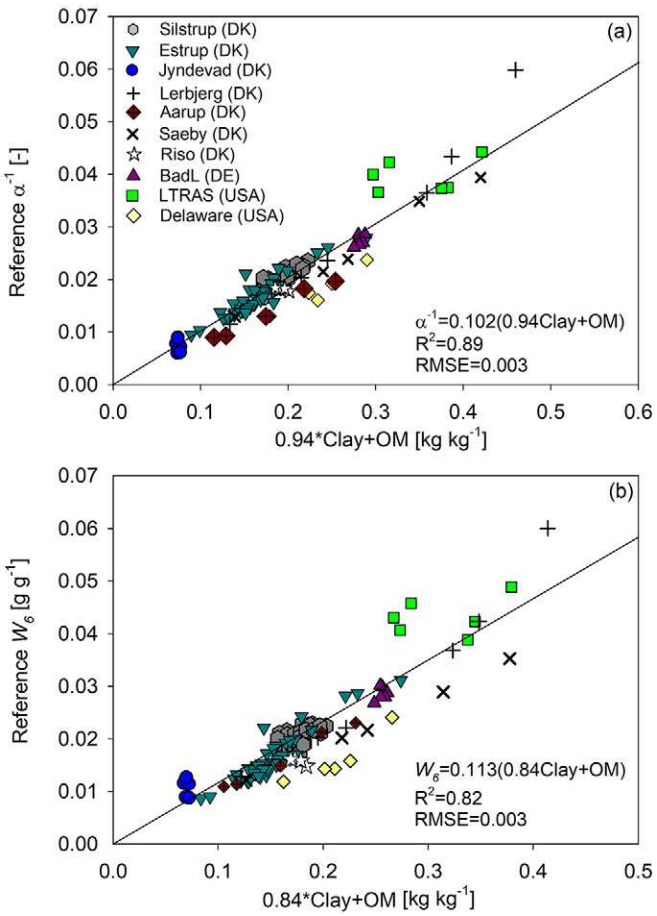

Fig. 7. Linear regression analyses of (a) the inverse of the slope of the Campbell–Shiozawa function (α^{-1}) and (b) the gravimetric water content at -10^6 cm H_2O (W_6) as a function of the clay content and organic matter (OM). Also given are the R^2 and RMSE between measured and predicted values.

Table 2. The results of partial least squares (PLS) regression analysis of visible–near-infrared (vis–NIR) spectra and linear regression analysis based pedotransfer function (PTF).

Model	Parameter†	R^2Cal‡	R^2CV§	RMSECV¶	RPIQ#	Factors or equation
Vis–NIRS	α^{-1}	0.76	0.72	0.0041	0.93	5
	W_6 (g g^{-1})	0.76	0.73	0.0042	0.92	5
PTF	α^{-1}	0.89	–	0.0025	1.66	$\alpha^{-1} = 0.102(0.94\text{Clay} + \text{OM})$
	W_6 (g g^{-1})	0.82	–	0.0034	1.15	$W_6 = 0.113(0.84\text{Clay} + \text{OM})$

† α, slope of the log-linear Campbell–Shiozawa function; W_6, water content at pF 6.
‡ R^2Cal, R^2 of the calibration dataset for the vis-NIRS model and R^2 of the equation for the PTF.
§ R^2CV, R^2 of the cross-validation dataset.
¶ RMSECV, root mean square error of the cross-validation dataset for the vis-NIRS model and root mean square error of the predicted parameters for the PTF.
# RPIQ, ratio of performance to interquartile distance.

Table 3. Statistical characteristics for the slope of the log-linear Campbell–Shiozawa function (α) and the gravimetric water content at pF 6 (W_6) for the whole dataset using visible–near-infrared spectroscopy (vis–NIRS) or pedotransfer function (PTF) based models.

Parameter	Model	Mean	Median	Q1	Q3	σ	Range
α	vis–NIRS	55.04	52.92	48.44	59.49	18.24	19.47–178.72
	PTF	55.71	53.71	47.41	59.01	20.70	21.304–136.0
W_6 (g g^{-1})	vis–NIRS	0.020	0.019	0.017	0.020	0.007	0.008–0.052
	PTF	0.020	0.019	0.017	0.021	0.007	0.008–0.047

Looking at Fig. 5 and 6 and the fact that the statistical evaluations of α and W_6 in Table 2 were very similar, we examined the relationship between them. The value of W_6 as a function of α^{-1} had a strong linear relationship because both parameters are strongly related to the clay content. The linear regression analysis showed $\alpha^{-1} = 1 \times W_6$ with $R^2 = 0.95$, $p < 0.001$, and standard error of the estimate equal to 0.006. Thus, the anchored log-linear CS function can be transformed into a one-parameter function instead of two parameters:

$$W = W_6(\text{pF}+5) \quad [10]$$

Comparison of this study with the literature is limited since there are no other studies that have attempted to predict the dry end of the SWRC using NIRS. However, a few studies have attempted to predict the SWRC at the wet end using vis–NIRS (Santra et al., 2009; Babaeian et al., 2015; Pittaki-Chrysodonta et al., 2018). Pittaki-Chrysodonta et al. (2018) predicted the Campbell soil-water retention function. In that study, they had anchored the original Campbell SWRC at pF 3 and developed vis–NIRS models to predict the Campbell b (pore-size distribution index) and the volumetric water content at pF 3 with R^2CV and RMSE equal to 0.86 and 0.92 and to 1.52 and 0.022 cm^3 cm^{-3}, respectively. Babaeian et al. (2015) developed point and parametric spectral transfer functions to predict soil-water content at specific matric potentials as well as the van Genuchten parameters (α_{VG} and n_{VG}) and the Brooks and Corey shape parameters (α_{BC} and λ_{BC}). The volumetric water content at the lowest matric potential that they predicted was at pF 4.2 with $R^2 = 0.63$ and RMSE = 0.0126 cm^3 cm^{-3}.

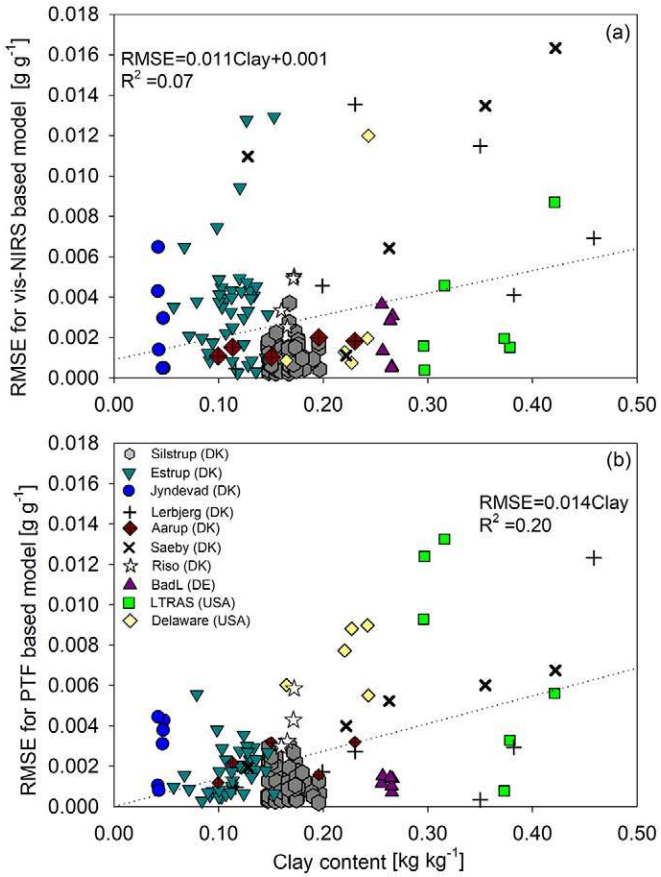

Fig. 8. Average RMSE values for predicted water vapor desorption isotherms from pF 5.5 to 6.5 (pF = log|ψ|) as a function of the clay content for (a) the visible–near-infrared spectroscopy (vis–NIRS) based model and (b) the pedotransfer function (PTF).

Pedotransfer Analysis

The linear regression analysis (Fig. 7a and b) showed that both parameters were linearly correlated with the clay and organic matter contents. High values of R^2 (0.89) and low values of the RMSE (0.0025) for predicting α^{-1} indicated a fairly good model development (Table 2). Arthur et al. (2013) predicted α^{-1} based only on knowledge of the clay content for 21 samples, with R^2 = 0.88. In this study, gradient soils (soils with approximately the same organic C contents but variable clay contents) were included and, for that reason, a PTF based only on the clay content would lead to poorer results (R^2 = 0.81, RMSE = 0.004). Schneider and Goss (2012) also correlated the inverse of the slope (α^{-1}) with the clay content using only 18 soil samples, with R^2 = 0.96.

The results from the prediction of W_6 using a PTF showed that it is also linearly related to the clay content and OM, with R^2 = 0.82 and RMSE = 0.0034 g g^{-1}, and this linearity can be observed in Fig. 7b. Jensen et al. (2015) correlated the volumetric water content at pF 6 with clay content (R^2 = 0.87). Furthermore, they found that including OM, silt, and bulk density increased the explained variation of the volumetric water content at pF 6 (R^2 = 0.95).

The statistical characteristics for the predicted parameters are given in Table 3. The PTF-predicted inverse of α and W_6 presented similar statistical characteristics to the reference except the maximum value of α^{-1}, which was underpredicted (136.00 instead of 165.54).

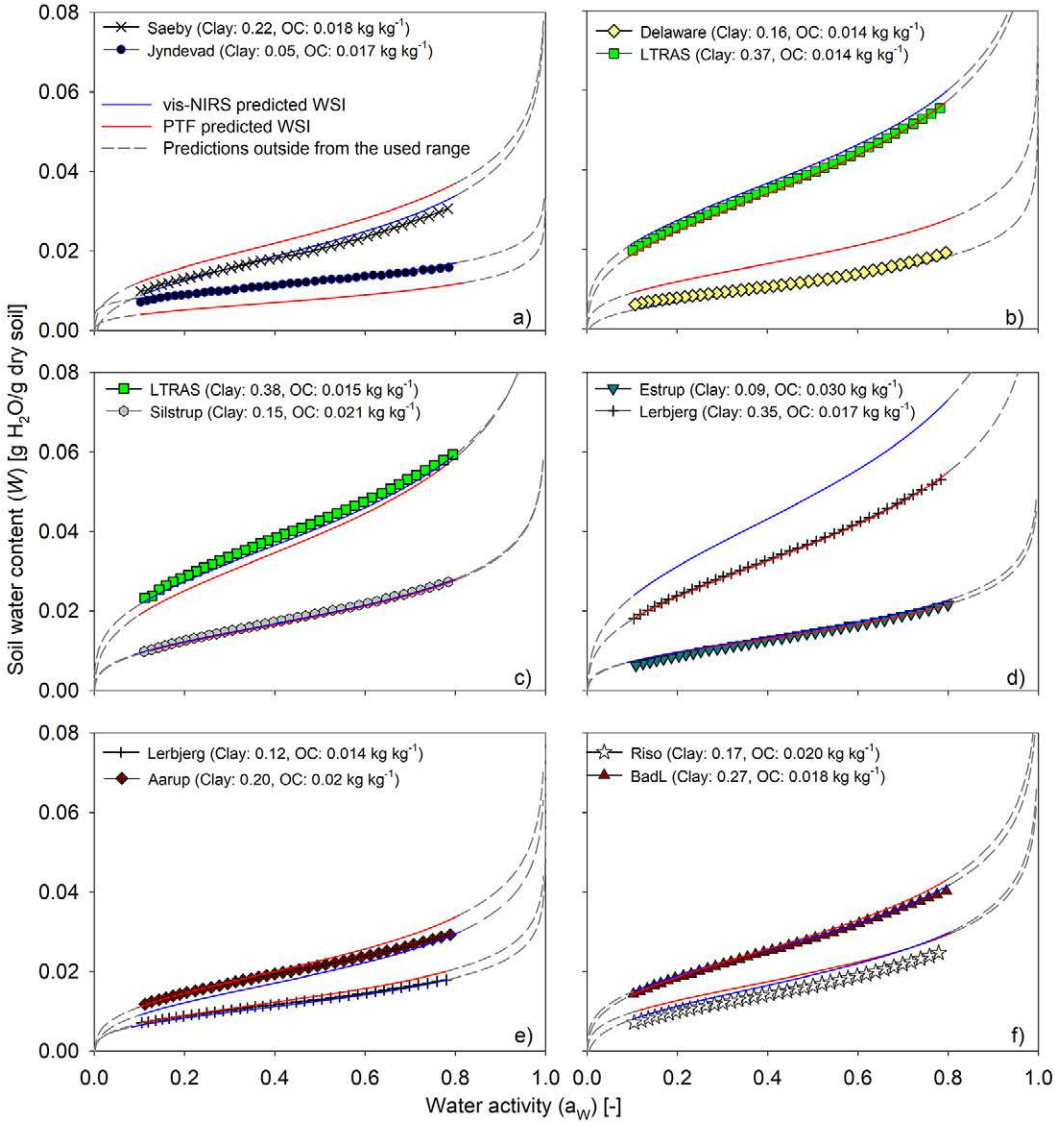

Fig. 9. Examples of the predictive performance of the water desorption isotherms (WSI) using visible–near-infrared spectroscopy (vis–NIRS) and pedotransfer function (PTF) models for eight soil samples with different clay and organic C (OC) contents: (a) Saeby (loam) and Jyndevad (sand), (b) Delaware (loam) and LTRAS (silty clay loam), (c) LTRAS (silty clay loam) and Silstrup (sandy loam), (d) Estrup (sandy loam) and Lerbjerg (sandy clay), (e) Lerbjerg (sandy loam) and Aarup (loam) and (f) Riso (sandy loam) and BadL (silty loam).

Comparison of Visible–Near-Infrared Spectroscopy Model and Pedotransfer Function

The two predicted parameters (α and W_6) from the vis–NIRS and PTF were inserted into the anchored log-linear CS function, and the entire dry end of the SWRC was predicted. Figure 8 shows the RMSE for gravimetric soil water content when predicting the SWRC from pF 5.5 to 6.5 as a function of clay content for both vis–NIRS and PTF models and the weak correlation between the clay content and the two models (R^2 0.07 and 0.20 for vis–NIRS and PTF, respectively).

To obtain the water desorption isotherms (WSIs), the predicted parameters α and W_6 using both methods (PTF and vis–NIRS) were inserted into the log-linear CS function anchored at pF 6. Thereafter, matric potentials (pF) at various gravimetric water contents were obtained using Eq. [5]. Afterward, the pF values were converted into water activity (a_w) using Eq. [1].

Examples of the predictive performance of 12 WSIs are depicted in Fig. 9, including at least one soil sample from each dataset. The two methods had similar prediction accuracy for soil samples from Silstrup, Aarup, Riso, and BadL. The vis–NIRS method had better accuracy for soil samples from LTRAS and Delaware, while the PTF was better for the Saeby, Estrup, and Jyndevad soils.

To evaluate the ability to predict the WSI across-field variations, the two fields from Estrup and Silstrup were used. The average predicted values of parameters for both methods (vis–NIRS and PTF) were inserted into the anchored log-linear CS function and the results are illustrated in Fig. 10. Both methods predicted well the WSI, with the vis–NIRS having slightly better accuracy based on the RMSE.

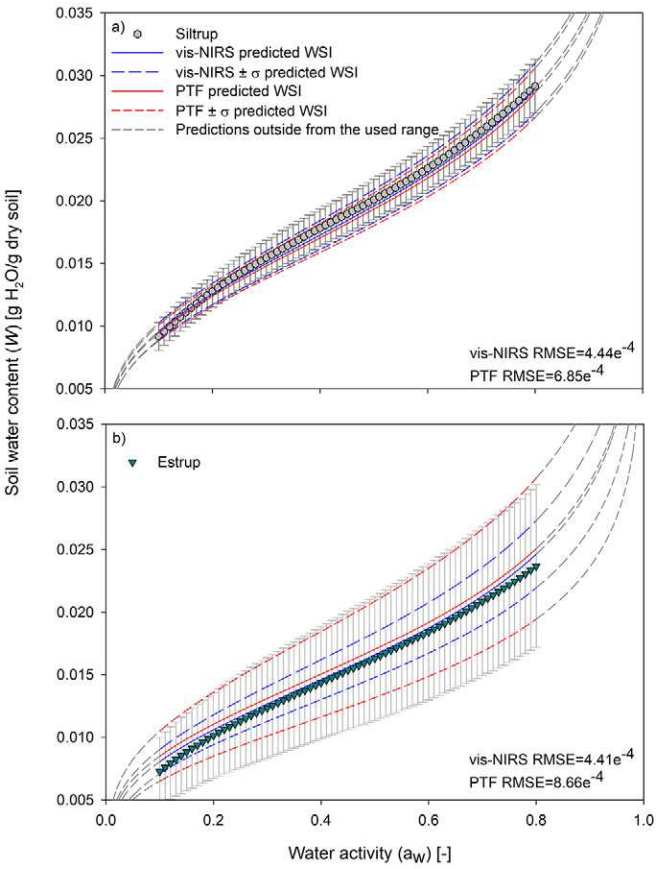

Fig. 10. Comparison between averaged measurements of water vapor sorption isotherms (WSI) (with vertical error bars) and the predicted WSI using visible–near-infrared spectroscopy (vis–NIRS) and pedotransfer function (PTF) models for the two fields: (a) Silstrup and (b) Estrup. Also given are the average RMSE values when predicting the vapor desorption isotherms using vis-NIRS and PTF based prediction models. Red and blue dashed lines indicate the possible predicted range (average ± σ). Gray dashed lines illustrate the predictions of WSI outside of the used range.

Conclusions

We examined whether vis–NIRS can predict the dry end of the SWRC equally well as a developed pedotransfer function. The log-linear CS function anchored at pF 6 was used, and its two parameters (α and W_6) were predicted using both methods (vis–NIRS and PTF).

Based on the R^2, RMSE, and RPIQ, the two CS parameters were best predicted using the PTF. The two predicted parameters were inserted into the anchored CS function and the predicted SWRC compared closely with the measurements for the majority of the soil samples. The ability to predict SWRC not only on individual soil samples but on the field scale was tested as well. Both methods predicted the SWRC with an acceptable accuracy for the two selected fields, with vis–NIRS performing slightly better.

Although this study included soil samples collected across Denmark, Germany, and the United States covering a wide textural distribution, more soil samples should be included from different geographical locations to test the applicability of vis–NIRS to an even wider range of soil types and to additionally enable an independent validation.

In further perspective, a tool to predict the entire SWRC from wet to hyper-dry from, e.g., a single vis–NIRS measurement would be highly useful for estimating plant-available water and improved simulations of water and chemical transport in variably saturated soil. This could be achieved by combining the dry-end concept of this study with a recent, analog concept for obtaining the wet end from vis–NIRS or PTF predicted parameters based on the Campbell (1974) retention model (Pittaki-Chrysodonta et al., 2018). Finally, a full-range SWRC model, e.g., that by Lu (2016), could be fitted to water retention from the wet end (Pittaki-Chrysodonta et al., 2018) and from the dry end (this study). Such an approach will be tested and independently validated in an upcoming study.

Acknowledgments

This research study was funded by an Aarhus University Research Foundation grant (AUFF-E-2016-9-36) and VILLUM FONDEN Research Grant 13162.

References

Arthur, E., M. Tuller, P. Moldrup, and L.W. de Jonge. 2014a. Evaluation of a fully automated analyzer for rapid measurement of water vapor sorption isotherms for applications in soil science. Soil Sci. Soc. Am. J. 78:754–760. doi:10.2136/sssaj2013.11.0481n

Arthur, E., M. Tuller, P. Moldrup, and L.W. de Jonge. 2014b. Rapid and fully automated measurement of water vapor sorption isotherms: New opportunities for vadose zone research. Vadose Zone J. 13(1). doi:10.2136/vzj2013.10.0185

Arthur, E., M. Tuller, P. Moldrup, D.K. Jensen, and L.W. de Jonge. 2015. Prediction of clay content from water vapour sorption isotherms considering hysteresis and soil organic matter content. Eur. J. Soil Sci. 66:206–217. doi:10.1111/ejss.12191

Arthur, E., M. Tuller, P. Moldrup, A.C. Resurreccion, M.S. Meding, K. Kawamoto, et al. 2013. Soil specific surface area and non-singularity of soil-water retention at low saturations. Soil Sci. Soc. Am. J. 77:43–53. doi:10.2136/sssaj2012.0262

Babaeian, E., M. Homaee, H. Vereecken, C. Montzka, A.A. Norouzi, and M.Th. van Genuchten. 2015. A comparative study of multiple approaches for predicting the soil-water retention curve: Hyperspectral information vs. basic soil properties. Soil Sci. Soc. Am. J. 79:1043–1058. doi:10.2136/sssaj2014.09.0355

Barnes, R.J., M.S. Dhanoa, and S.J. Lister. 1989. Standard normal variate transformation and de-trending of near-infrared diffuse reflectance spectra. Appl. Spectrosc. 43:772–777. doi:10.1366/0003702894202201

Bellon-Maurel, V., E. Fernandez-Ahumada, B. Palagos, J.M. Roger, and A. McBratney. 2010. Critical review of chemometric indicators commonly used for assessing the quality of the prediction of soil attributes by NIR spectroscopy. TrAC Trends Anal. Chem. 29:1073–1081. doi:10.1016/j.trac.2010.05.006

Brown, D.J., R.S. Bricklemyer, and P.R. Miller. 2005. Validation requirements for diffuse reflectance soil characterization models with a case study of VNIR soil C prediction in Montana. Geoderma 129:251–267. doi:10.1016/j.geoderma.2005.01.001

Brunauer, S., P.H. Emmett, and E. Teller. 1938. Adsorption of gases in multimolecular layers. J. Am. Chem. Soc. 60:309–319. doi:10.1021/ja01269a023

Campbell, G.S. 1974. Simple method for determining unsaturated conductivity from moisture retention data. Soil Sci. 117:311–314. doi:10.1097/00010694-197406000-00001

Campbell, G.S., and S. Shiozawa. 1992. Prediction of hydraulic properties of soils using particle-size distribution and bulk density data. In: M.Th. van Genuchten et al., editors, Proceedings of the International Workshop on Indirect Methods for Estimating the Hydraulic Properties of Unsaturated Soils, Riverside, CA. 11–13 Oct. 1989. US Salinity Lab., Riverside, CA. p. 317–328.

Chen, C., T.S. Ren, K.L. Hu, B.G. Li, and Y.J. Wang. 2014. Estimation of soil clay content using hygroscopic water content at an arbitrary humidity. Soil Sci. Soc. Am. J. 78:119–124. doi:10.2136/sssaj2013.06.0247

Ciocca, F., I. Lunati and M.B. Parlange. 2014. Effects of the water-retention curve on evaporation from arid soils. Geophys. Res. Lett. 41:3110–3116. doi:10.1002/2014GL059827

de Jong, S. 1993. Simpls: An alternative approach to partial least-squares regression. Chemom. Intell. Lab. Syst. 18:251–263. doi:10.1016/0169-7439(93)85002-X

de Jonge, L.W., P. Moldrup, and P. Schjonning. 2009. Soil infrastructure, interfaces & translocation processes in inner space ("Soil-it-is"): Towards a road map for the constraints and crossroads of soil architecture and biophysical processes. Hydrol. Earth Syst. Sci. 13:1485–1502. doi:10.5194/hess-13-1485-2009

Dexter, A.R., G. Richard, D. Arrouays, E.A. Czyz, C. Jolivet, and O. Duval. 2008. Complexed organic matter controls soil physical properties. Geoderma 144:620–627. doi:10.1016/j.geoderma.2008.01.022

Eden, M., P. Moldrup, P. Schjonning, H.J. Vogel, K.M. Scow, and L.W. de Jonge. 2012. Linking soil physical parameters along a density gradient in a loess-soil long-term experiment. Soil Sci. 177:1–11. doi:10.1097/SS.0b013e31823745a9

Fayer, M.J., and C.S. Simmons. 1995. Modified soil-water retention functions for all matric suctions. Water Resour. Res. 31:1233–1238. doi:10.1029/95WR00173

Galvão, L.S., and I. Vitorello. 1998. Variability of laboratory measured soil lines of soils from southeastern Brazil. Remote Sens. Environ. 63:166–181. doi:10.1016/S0034-4257(97)00135-1

Gee, G.W., and D. Or. 2002. Particle-size analysis. In: J.H. Dane and C.G. Topp, editors, Methods of soil analysis. Part 4. Physical methods. SSSA Book Ser. 5. SSSA, Madison, WI. p. 255–293. doi:10.2136/sssabookser5.4.c12

Gowen, A.A., G. Downey, C. Esquerre, and C.P. O'Donnell. 2011. Preventing over-fitting in PLS calibration models of near-infrared (NIR) spectroscopy data using regression coefficients. J. Chemometr. 25:375–381. doi:10.1002/cem.1349

Groenevelt, P.H., and C.D. Grant. 2004. A new model for the soil-water retention curve that solves the problem of residual water contents. Eur. J. Soil Sci. 55:479–485. doi:10.1111/j.1365-2389.2004.00617.x

Hermansen, C., M. Knadel, P. Moldrup, M.H. Greve, D. Karup, and L.W. de Jonge. 2017. Complete soil texture is accurately predicted by visible near-infrared spectroscopy. Soil Sci. Soc. Am. J. 81: 758–769. doi:10.2136/sssaj2017.02.0066

Hunt, G.R. 1977. Spectral signatures of particulate minerals in visible and near infrared. Geophysics 42:501–513. doi:10.1190/1.1440721

Jensen, D.K., M. Tuller, L.W. de Jonge, E. Arthur, and P. Moldrup. 2015. A new two-stage approach to predicting the soil water characteristic from saturation to oven-dryness. J. Hydrol. 521:498–507. doi:10.1016/j.jhydrol.2014.12.018

Karup, D., P. Moldrup, M. Tuller, E. Arthur, and L.W. de Jonge. 2017. Prediction of the soil water retention curve for structured soil from saturation to oven-dryness. Eur. J. Soil Sci. 68:57–65. doi:10.1111/ejss.12401

Katuwal, S., C. Hermansen, M. Knadel, P. Moldrup, M.H. Greve, and L.W. de Jonge. 2017. Combining X-ray computed tomography and visible near-infrared spectroscopy for prediction of soil structural properties. Vadose Zone J. 17:160054. doi:10.2136/vzj2016.06.0054

Khlosi, M., W.M. Cornelis, A. Douaik, M.Th. van Genuchten, and D. Gabriels. 2008. Performance evaluation of models that describe the soil water retention curve between saturation and oven dryness. Vadose Zone J. 7:87–96. doi:10.2136/vzj2007.0099

Knadel, M., F. Masis-Melendez, L.W. de Jonge, P. Moldrup, E. Arthur and M.H. Greve. 2016. Assessing soil water repellency of a sandy field with visible near infrared spectroscopy. J. Near Infrared Spectrosc. 24:215–224. doi:10.1255/jnirs.1188

Lu, N. 2016. Generalized soil water retention equation for adsorption and capillarity. J. Geotech. Geoenviron. Eng. 142(10). doi:10.1061/(ASCE)GT.1943-5606.0001524

Lu, N., and M. Khorshidi. 2015. Mechanisms for soil-water retention and hysteresis at high suction range. J. Geotech. Geoenviron. Eng. 141(8). doi:10.1061/(ASCE)GT.1943-5606.0001325

Masís-Meléndez, F., T.K.K. Chamindu Deepagoda, L.W. de Jonge, M. Tuller, and P. Moldrup. 2014. Gas diffusion-derived tortuosity governs saturated hydraulic conductivity in sandy soils. J. Hydrol. 512:388–396. doi:10.1016/j.jhydrol.2014.02.063

Norgaard, T., P. Moldrup, P. Olsen, A.L. Vendelboe, B.V. Iversen, M.H. Greve, et al. 2013. Comparative mapping of soil physical-chemical and structural parameters at field scale to identify zones of enhanced leaching risk. J. Environ. Qual. 42:271–283. doi:10.2134/jeq2012.0105

Norris, K. 2001. Applying Norris derivatives: Understanding and correcting the factors which affect diffuse transmittance spectra. NIR News 12:6–9. doi:10.1255/nirn.613

Or, D., and M. Tuller. 1999. Liquid retention and interfacial area in variably saturated porous media: Upscaling from single-pore to sample-scale model. Water Resour. Res. 35:3591–3605. doi:10.1029/1999WR900262

Oswin, C.R. 1946. The kinetics of package life: III. The isotherm. J. Soc. Chem. Ind. 65:419–421. doi:10.1002/jctb.5000651216

Paradelo, M., C. Hermansen, M. Knadel, P. Moldrup, M.H. Greve and L.W. de Jonge. 2016. Field-scale predictions of soil contaminant sorption using visible–near infrared spectroscopy. J. Near Infrared Spectrosc. 24:281–291. doi:10.1255/jnirs.1228

Paradelo, M., T. Norgaard, P. Moldrup, T.P.A. Ferré, K.G.I.D. Kumari, E. Arthur, and L.W. de Jonge. 2015. Prediction of the glyphosate sorption coefficient across two loamy agricultural fields. Geoderma 259–260:224–232. doi:10.1016/j.geoderma.2015.06.011

Peleg, M. 1993. Assessment of a semi-empirical four parameter general model for sigmoid moisture sorption isotherms. J. Food Process Eng. 16:21–37. doi:10.1111/j.1745-4530.1993.tb00160.x

Pittaki-Chrysodonta, Z., P. Moldrup, M. Knadel, B.V. Iversen, C. Hermansen, M.H. Greve, and L.W. de Jonge. 2018. Predicting the Campbell soil water retention function: Comparing visible–near-infrared spectroscopy with classical pedotransfer function. Vadose Zone J. 17:170169. doi:10.2136/vzj2017.09.0169

Reeves, J.B., G.W. McCarty, and J.J. Meisinger. 1999. Near infrared reflectance spectroscopy for the analysis of agricultural soils. J. Near Infrared Spectrosc. 7:179–193. doi:10.1255/jnirs.248

Ross, P.J., J. Williams, and K.L. Bristow. 1991. Equation for extending water-retention curves to dryness. Soil Sci. Soc. Am. J. 55:923–927. doi:10.2136/sssaj1991.03615995005500040004x

Rossi, C., and J.R. Nimmo. 1994. Modeling of soil-water retention from saturation to oven dryness. Water Resour. Res. 30:701–708. doi:10.1029/93WR03238

Santra, P., R.N. Sahoo, B.S. Das, R.N. Samal, A.K. Pattanaik, and V.K. Gupta. 2009. Estimation of soil hydraulic properties using proximal spectral reflectance in visible, near-infrared, and shortwave-infrared (VIS–NIR–SWIR) region. Geoderma 152:338–349. doi:10.1016/j.geoderma.2009.07.001

Savitzky, A., and M.J.E. Golay. 1964. Smoothing and differentiation of data by simplified least squares procedures. Anal. Chem. 36:1627–1639. doi:10.1021/ac60214a047

Schneider, M., and K.U. Goss. 2012. Prediction of the water sorption isotherm in air dry soils. Geoderma 170:64–69. doi:10.1016/j.geoderma.2011.10.008

Snee, R.D. 1977. Validation of regression models: Methods and examples. Technometrics 19:415–428. doi:10.1080/00401706.1977.10489581

Stenberg, B., R.A. Viscarra Rossel, A.M. Mouazen, and J. Wetterlind. 2010. Visible and near infrared spectroscopy in soil science. Adv. Agron. 107:163–215. doi:10.1016/S0065-2113(10)07005-7

Tuller, M., and D. Or. 2005. Water films and scaling of soil characteristic curves at low water contents. Water Resour. Res. 41:W09403. doi:10.1029/2005WR004142

van den Berg, C., and S. Bruin. 1981. Water activity and its estimation in food systems: Theoretical aspects. In: L.B. Rockland and G.F. Stewart, editors, Water activity: Influences on food quality. Academic Press, New York. p. 1–61. doi:10.1016/B978-0-12-591350-8.50007-3

van Genuchten, M.Th. 1980. A closed-form equation for predicting the hydraulic conductivity of unsaturated soils. Soil Sci. Soc. Am. J. 44:892–898. doi:10.2136/sssaj1980.03615995004400050002x

Vendelboe, A.L., P. Moldrup, P. Schjonning, D.J. Oyedele, Y. Jin, K.M. Scow, and L.W. de Jonge. 2012. Colloid release from soil aggregates: Application of laser diffraction. Vadose Zone J. 11(1). doi:10.2136/vzj2011.0070

Webb, S.W. 2000. A simple extension of two-phase characteristic curves to include the dry region. Water Resour. Res. 36:1425–1430. doi:10.1029/2000WR900057

Wuddivira, M.N., D.A. Robinson, I. Lebron, L. Brechet, M. Atwell, S. De Caires, et al. 2012. Estimation of soil clay content from hygroscopic water content measurements. Soil Sci. Soc. Am. J. 76:1529–1535. doi:10.2136/sssaj2012.0034